

Tropical cyclones facilitate recovery of forest leaf area from dry spells in East Asia

Yi-Ying Chen¹ and Sebastiaan Luyssaert²

¹Research Center for Environmental Changes, Academia Sinica, Taipei, 11529, Taiwan

²Amsterdam Institute for Life and Environment, Vrije Universiteit Amsterdam, Amsterdam, 1081, The Netherlands

Correspondence to: Yi-Ying Chen (yiyingchen@gate.sinica.edu.tw)

Abstract. Forests disturbance by tropical cyclones is mostly documented by field studies of exceptionally strong cyclones and satellite-based approaches attributing decreases in leaf area. By starting their analysis from the observed damage, these studies are biased and may, therefore, limit our understanding of the impact of cyclones in general. This study overcomes such biases by jointly analysing the cyclone tracks, climate reanalysis, and changes in satellite-based leaf area following the passage of 140 ± 41 cyclones. Sixty days following their passage, $18 \pm 8\%$ of the cyclones resulted in a decrease and $48 \pm 18\%$ showed no change in leaf area compared to nearby forest outside the storm track. For a surprising $34 \pm 7\%$ of the cyclones, an increase in leaf area was observed. Cyclones resulting in higher leaf area in their affected compared to their reference area coincided with an atmospheric pressure dipole steering the cyclone towards a region experiencing a dry spell caused by the same dipole. When the dipole was present, the destructive power of cyclones was offset by their abundant precipitation enabling forest canopies in the affected area to recover faster from the dry spell than canopies in the reference area. This study documents previously undocumented widespread antagonist interactions on forest leaf area between tropical cyclones and droughts.

Main Text

Each year almost 30 cyclones, about one-third of the world's tropical cyclones, develop over the Pacific Ocean north of the equator (Landsea, 2000) where a subtropical ridge steers them mainly west and northwest towards Eastern Asia, where 90% make landfall. The majority of the tropical cyclones in the north western Pacific basin develop between June and November (Bushnell et al., 2018) and more than half acquire typhoon strength (WMO, 2017). Although natural ecosystems, such as forests, have adapted to recurring high wind speeds (Eloy et al., 2017; Louf et al., 2018; Curran et al., 2008), stem breakage is almost unavoidable at wind speeds above 40 ms^{-1} (Virot et al., 2016) but has been widely reported at wind speeds well below this threshold together with other damage (Tang et al., 2003; Chiu et al., 2018; Chang et al., 2020).

By jointly analysing cyclone tracks (Joint Typhoon Warning Center; JTWC, 2019), climate reanalysis data (ERA5-Land; ECMWF, 2019), satellite-based proxies of soil dryness (SPEIbase v2.6; Beguería et al., 2014), land cover (ESA CCI; ESA, 2017), and leaf area (ESA LAI; Martins et al., 2020), we estimated: (a) the impact of tropical cyclones on leaf area, and (b) the main drivers of this impact. Previous studies attributed decreases in leaf area or related satellite-

33 based indices to different disturbance agents (Ozdogan et al., 2014; Honkavaara et al., 2013; Forzieri et al., 2020),
34 including cyclones (Takao et al., 2014). A damage-based approach is designed to identify only decreases in leaf area,
35 thus failing to identify events in which tropical cyclones left the leaf area unaltered or even increased it. In contrast,
36 this study starts the analysis from the actual storm tracks which allows for an unbiased assessment of the impact of
37 cyclones on forests (Blanc and Strobl, 2016).

38
39 The land area affected was identified for each of the 580 tropical cyclones that occurred in the study region between
40 1999 and 2018, considering that cyclone-driven damage could only occur within the storm track at locations that
41 experienced high wind speeds or high precipitation. Pixels within the storm track defined as two, three, or four times
42 the diameter of the cyclone for which threshold values for wind or precipitation were exceeded were classified as
43 affected areas (**Fig. A1**), the remaining pixels in the track served as a cyclone-specific reference area. The uncertainty
44 derived from defining the width of the storm track (Willoughby and Rahn, 2004) and determining which wind speeds
45 and amounts of precipitation could result in damage are accounted for by an ensemble of nine related definitions with
46 different threshold values (**Table A1**). In this study uncertainties represent the standard deviation across the nine
47 definitions for the affected area and are shown in **Figs 1, 2c A1, and A3**.

48
49 The impact of a tropical cyclone on leaf area was calculated based on the adjusted Hedge's effect size by comparing
50 the change in leaf area before and after the cyclone in the affected area with the change before and after the cyclone
51 in the reference area for each individual cyclone (**Eq. 1**). Using a reference area that is specific to each cyclone means
52 that seasonal dynamics related to leaf phenology and seasonal monsoons are accounted for in the effect size, which is
53 a unitless description of the mean change in leaf area normalized by its standard deviation (**Eq. 1**). Hence, a positive
54 effect size denotes a faster increase (or a slower decrease) in leaf area in the affected area compared to the reference
55 area following the passage of a tropical cyclone.

56
57 A total of 316 ± 22 tropical cyclones or $54 \pm 4\%$ of the storm events under study could not be further analysed (**Table**
58 **A1**) because leaf area index observations were missing from either the affected area, the reference area, or both, thus
59 violating the requirements for calculating the effect size (**Eq. 1**). Of the remaining 264 ± 22 tropical cyclones, only
60 140 ± 41 passed the additional quality check necessary to be retained for further analysis in this study, i.e., the difference
61 in the leaf area between the reference and affected area prior to the passage of a storm should be less than 10% of the
62 leaf area in the reference area. In other words, prior to the storm, the leaf area in the reference area had to be similar
63 to the leaf area in what will become the affected area once the storm passed. Of the 580 cyclones, 31% was less than
64 class I, 14% was classified as class I, 11% as class II, 10% as class III, 21 % as class IV, and 13% as class V. The
65 distribution of the intensity classes of the sample of 140 ± 41 cyclones that could be further analysed were similar to
66 the census of the 580 cyclones (**Fig. A3**). Despite the loss of around 75% of the events, the sample analysed in this
67 study was unbiased in terms of cyclone intensity classes (**Fig. A3**).

68

69 Tropical cyclones have been widely observed to defoliate and disturb forests (Wang et al., 2013; Uriarte et al., 2019;
70 Chambers et al., 2007; Douglas, 1999; Lin et al., 2011). Nevertheless, in this study, only $18\pm 8\%$ of the observed
71 cyclones resulted in a detectable reduction in leaf area 60 days after their passage as a direct effect of limb breaking,
72 uprooting, stem breakage, and landslides following high wind speeds and heavy precipitation. For $48\pm 18\%$ of the
73 cyclones, the change in leaf area 60 days after a cyclone passed was so small that it could not be distinguished from
74 the threshold representing no-change. Ecological theory predicts forest dwarfing in regions with high cyclone
75 frequencies compared to the longevity of a tree, directly through gradual removal of taller trees over many generations
76 (Lin et al., 2020; McDowell et al., 2020) and indirectly through the loss of nutrients (Tang et al., 2003; Lin et al.,
77 2011). Where forest dwarfing has occurred, it might be hard to observe the short-term effects of an individual tropical
78 cyclone on forest structure and function (Mabry et al., 1998).

79
80 For a surprising $34\pm 7\%$ of the cyclones an increase or given the way the effect size was calculated, a reduced decrease
81 in leaf area was observed, leading to the question which conditions could explain such an increase (or reduced
82 decrease)? Following Liebig's law of the minimum (Chapin III et al., 2011), the observed increase (or reduced
83 decrease) in leaf area implies that about one-third of the cyclones alleviated one or more growth factors that were
84 limiting leaf area prior to the passage of the cyclones. We hypothesize that a dry spell could be the growth limiting
85 factor prior to the cyclone, whereas the precipitation brought by the cyclone could enhance plant growth through
86 mitigating soil dryness.

87
88 To test this hypothesis, the standardized precipitation and evapotranspiration index prior to 60-days following the
89 passage of the cyclone, the accumulated precipitation prior to the cyclone, and the accumulated precipitation brought
90 by the cyclone were determined for each of the 140 ± 41 tropical cyclones that passed the quality checks. An increase
91 (or reduced decrease) in leaf area was observed for cyclones that made landfall during a dry spell and brought sufficient
92 precipitation to increase the standardized precipitation and evapotranspiration index (**Fig. 1a**) supporting our
93 hypothesis. The hypothesis was further supported no change in leaf area for cyclones making landfall when plant
94 water demand was satisfied by soil moisture availability shown by the standardized precipitation and
95 evapotranspiration index approaching zero (**Fig. 1a**). Furthermore, decreases in leaf area 60 days following the cyclone
96 were observed for cyclones making landfall when there was an excess in plant available water (**Fig. 1a**).

97
98 Where a dry spell prior to the cyclone in combination with the precipitation brought by the cyclone provides a
99 mechanistic explanation for increased plant growth following the passage of a tropical cyclone, the abundance of such
100 events (i.e., $34\pm 7\%$) suggests a non-random relationship between the location and timing of dry spells and cyclones
101 (**Fig. 2c**). For the mid-latitudes, dry summers see indeed an increase in the number of tropical cyclones making landfall
102 which often ends the summer drought (Yoo et al., 2015). In South Korea, for example, at least 43% but possibly as
103 much as 90% of the summer droughts in coastal regions were abruptly ended by a tropical cyclone (Yoo et al., 2015).
104 The co-occurrence of dry spells and tropical cyclones has been linked to a meridional dipole system in the mid-latitude

105 regions of East Asia with a high-pressure system in the region of 40-50N and 150-160E where it is causing the dry
106 spell and the low-pressure system in the region of 20-30N and 120-150E.

107

108 To confirm the relationship between dry spells and the occurrence of cyclones, the meta-data for each of the 140±41
109 tropical cyclones was extended, resulting in the first group of meta-data of six characteristics describing the land
110 surface mainly before the passage of a cyclone and a second group containing five characteristics of the cyclone itself.
111 Following combined factorial analysis to identify collinearity between the land surface characteristics, cyclone
112 characteristics, and effect sizes (**Table A2**), the four main factors which explained 58% of the variance, were used in
113 a decision tree (**Fig. A4**) to create three cyclone groups (**Table 1**).

114

115 Sixty-two percent of the cyclones which were generated when the meridional dipole was present (indicated by a
116 negative Pacific Japan index (Nitta, 1987), making landfall at mid latitudes during a dry spell, and bringing sufficient
117 precipitation to rewet the soil and end the dry episode, increased the leaf area (or reduced the decrease) in the affected
118 compared to the reference area (cyclone group 1; **Table 1**). When the dipole is in place, tropical cyclones generated
119 from the monsoon trough over the West Pacific Ocean are steered through the trough in between the high- and low-
120 pressure systems towards and then along the coast of East Asia (Choi et al., 2010). While traveling along the edges of
121 the high pressure system, the tropical cyclone may disturb the circulation, resulting in an unfavourable environment
122 to sustain the dipole (Choi et al., 2011; Kubota et al., 2016) and bringing precipitation to the dry region that was under
123 the high pressure system.

124

125 Group 2 cyclones made landfall at low latitudes when the meridional dipole was in place and brought abundant
126 precipitation which increased soil wetness (**Table 1**). Given that under the meridional dipole, the dry spell occurs
127 under the high pressure system typically located between 40 and 50 N, but that many of the group 2 cyclones made
128 landfall at lower latitudes (i.e., $23.3\pm 6.9N$), chances to end a dry spell were lower which was reflected in the almost
129 equal chance to increase the leaf area (48%) or had an effect that could not be detected by our method (44%; **Table**
130 **1**). Nevertheless, the mechanistic relationship between soil dryness, precipitation, and change in leaf area was
131 confirmed for also this group (**Fig. 1b-d**).

132

133 Almost 60% of the tropical cyclones studied were classified as group 3 cyclones making them the most abundant type
134 of cyclone in the study region. Although 57% of the cyclones in this group resulted in no effect on leaf area (**Table**
135 **1**), this group contained about one third of the cyclones resulting in a positive effect on leaf area (**Table 1**) which
136 occurred when the soil was dry and the cyclone brought sufficient precipitation to rewet the soil (**Fig. 1b-d**).

137

138 Analysing the atmospheric pressure separately for cyclones that resulted in no change, an increase, or a decrease in
139 leaf area (**Fig. 3**) showed that tropical cyclones that were followed by an increase (or reduced decrease) in leaf area
140 coincided with a meridional dipole (**Fig. 3b**). Moreover, the genesis of tropical cyclones that were followed by a

141 decrease in leaf area, occurred under very different atmospheric conditions compared to cyclones followed by an
142 increasing leaf area (**Fig. 3c**). A relationship between the atmospheric system causing dry spells, tropical cyclones and
143 their subsequent impact on leaf areas, suggest that whether more drought damage is to be expected in the future will
144 not only depend on an increase in drought frequency and intensity but will in part be determined by the weather system
145 that is causing the drought. Although the co-occurrence of droughts and cyclones has previously been demonstrated
146 (Choi et al., 2011; Kubota et al., 2016), we believe this study to be the first to document its large-scale antagonist
147 effect on forest leaf area.

148
149 By studying a representative sample of tropical cyclones in terms of storm intensity, we showed that almost half of
150 the tropical cyclones, i.e., $48\pm 18\%$, caused little to no damage to forest leaf area, suggesting that forest dwarfing is a
151 general structural adaption in the study region. Moreover, a third, i.e., $34\pm 7\%$ of the cyclones in East Asia resulted in
152 an increase (or reduced decrease) in forest growth, because these storms relieved water stress within their track or
153 even ended dry spells. Remarkably, precipitation brought by a cyclone appeared as a more powerful predictor than
154 cyclone intensity when it comes to the vegetation response (**Table 1; Fig. A3**). The observed frequency of positive
155 vegetation responses to cyclones suggests that the present day vision of cyclones as agents of destruction (Altman et
156 al., 2018; Negrón-Juárez et al., 2010, 2014) should be refined toward a recognition that, depending on the
157 environmental conditions prior to the storm and the atmospheric conditions leading to the genesis of the tropical
158 cyclone, cyclones frequently facilitate the recovery of forest leaf area and as such dampen the effects of dry spells.

159

160 **Materials and Methods**

161 **Cyclone track and track diameter**

162 Since 1945, tropical cyclones in the Western North Pacific Ocean have been tracked and their intensity recorded by
163 the Joint Typhoon Warning Center (JTWC). The track data shared by the Joint Typhoon Warning Center consist of
164 quality-controlled six-hourly geolocation observations of the center of the storm with the diameter of the storm being
165 a proxy for its intensity (JTWC, 2019). For the period under consideration, from 1999 to 2018, the geolocations and
166 diameters are the output of the Dvorak model (Dvorak, 1984; Dvorak et al., 1990) derived from visible and infrared
167 satellite imagery. Storm diameters are available starting from January 2003. Prior to this date a generic diameter of
168 100 km (Lin et al., 2020) is used in this study. Linear interpolation of the six-hourly track data resulted in hourly track
169 data to fill in any gaps in the mapping of the cyclone track.

170

171 In this study, we focus on East Asia which, given the absence of natural boundaries, is defined as the land contained
172 within the north western Pacific basin that, according to the Joint Typhoon Warning Center stretches from 100 to 150
173 degrees east and 0 to 60 degrees north. The Joint Typhoon Warning Center compiled track and intensity data for 580
174 tropical cyclones between 1999 and 2018 in the north western Pacific basin. A shorter time series (1999 to 2018) than
175 the entire length of time available (1945 to 2018) was analysed due to the more limited availability of the leaf area

176 index data which had to be jointly analysed with the track and intensity data to quantify the impact of cyclones on
177 natural ecosystems.

178

179 **Area affected by individual cyclones**

180 The land area thought to be affected by a specific cyclone as well as the reference area for each of the 580 cyclones
181 that occurred in the study area between 1999 and 2018 were identified based on nine different but related definitions
182 (**Table A1**). Each definition comprises a combination of at least two out of three criteria, e.g., the diameter of the
183 cyclone, the maximum wind speed at each location during the passage of the cyclone, and accumulated precipitation
184 at each location during the passage of the cyclone. Each forested pixel within each individual storm track was classified
185 as either an affected area or a reference area based on these nine definitions. Differences in the results coming from
186 differences in the definitions were used throughout the analysis to estimate semantic uncertainties. Uncertainties
187 related to the estimated diameter of the cyclone, wind speed, and precipitation data were not accounted for in the
188 calculation of the affected and reference areas because they were thought to be smaller than the uncertainty coming
189 from differences in the definitions themselves.

190

191 The underlying assumption behind the definitions is that forests can only be affected by a specific cyclone if they are
192 located along its storm track. The minimum width of each storm track is the diameter of the cyclone as reported by
193 the Joint Typhoon Warning Center. Following the observation that over the ocean, the actual wind speed exceeds the
194 critical wind speed for stem breakage or uprooting (i.e., 17 m s^{-1} ref. Chen et al., 2018) over a distance of at least three
195 times the diameter of the cyclone (Willoughby and Rahn, 2004), the minimum width of a storm track in which cyclone-
196 related forest damage could occur is defined as three times the diameter recorded by the Joint Typhoon Warning
197 Center although wind speeds drop dramatically when cyclones make landfall (Kaplan and Demaria, 2001). The
198 minimum width of a storm track over land should, therefore, be reduced compared to the observations over the ocean.
199 This study used three different widths to define a storm track, i.e., two, three, or four times the recorded diameter
200 (**Table A1**).

201

202 Being located within the track of a specific cyclone is essential but not sufficient for damage to occur. Within a storm
203 track, only forested pixels that experienced high wind speeds or high precipitation were counted as in the potentially
204 affected area. Forest pixels that were located within the storm track but did not experience high wind speeds or high
205 precipitation were counted as in the reference area. Note that to better account for the uncertainties arising from this
206 approach, the threshold values for wind speed and precipitation were increased as the track diameter increased (**Table**
207 **A1**). For a narrow storm track, it is reasonable to assume that there would be damage shown in all pixels except those
208 where wind speed or precipitation did not exceed a relatively low threshold value. For wide storm tracks the opposite
209 applies; it is reasonable to assume that few of the pixels would show damage except where wind speed or precipitation
210 exceeded relatively high threshold values.

211

212 Wind speed and precipitation data were extracted from the ERA5-Land reanalysis data for land (ECMWF, 2019). The
213 ERA5-Land reanalysis dataset has a spatial resolution of 9 km x 9 km and a time step of 1 hour. It is the product of a
214 data assimilation study conducted with the H-TESEL scheme by ERA5 IFS Cy45r1 and nudged by climatological
215 observations (ECMWF, 2018). The Cy45r1 reanalysis dataset shows statistically neutral results for the position error
216 of individual cyclones (ECMWF Confluence Wiki: Implementation of IFS cycle 45r1). The spatial representation of
217 the reanalysis data is reported to compare favourably with observational data (Chen et al., 2021) outside the domain
218 of this study. No reports on similar tests for the current study domain, i.e., East Asia, were found. Furthermore, land
219 cover maps released through the European Space Agency's Climate Change Initiative (ESA, 2017) were used to
220 restrict the analysis to forests. The Climate Change Initiative maps integrate observations from several space-borne
221 sensors, including MERIS, SPOT-VGT, AVHRR, and PROBA-V, into a continuous map with a 300 m resolution
222 from 1994 onwards.

223
224 Wind speed and precipitation data were spatially disaggregated and temporally aggregated to match the spatial and
225 temporal resolution of the leaf area index product (see below). Maximum wind speed and accumulative precipitation
226 were aggregated over time steps to match the 10-day resolution of the leaf area index product. We preserved the
227 temporal resolution of the land cover map but aggregated its spatial resolution from 300 m to 1 km to match the
228 resolution of the leaf area index product. During aggregation, the majority of land cover at the 300 m resolution was
229 assigned to the 1 km pixel resolution.

230 231 **Impact on leaf area of an individual cyclone**

232 Version 2 of European Space Agency's Climate Change Initiative product was used to calculate leaf area in this study.
233 The product has a 1 km spatial resolution, and a 10-day temporal resolution, and is available from 1999 onwards. The
234 default leaf area index product is distributed as a composite image using at least six valid observations on a pixel
235 within a 30-day moving window (Verger et al., 2014). The composite image is drawn from satellite-based observations
236 of the surface reflectance in the red, near-infrared, and shortwave infrared from SPOT-VGT (from 1999 to May 2014)
237 and PROBA-V (from June 2014 to present). Gaps in missing observations are filled by the application of a relationship
238 between local weather and leaf area index dynamics. Gap filling resulted in errors on the leaf area index estimates of
239 less than 0.18 (Martins et al., 2017). The spatiotemporal resolution of the leaf area index products was the coarsest of
240 all data products used and therefore determined the spatiotemporal resolution of the analysis as a whole. Moreover,
241 the availability of the leaf area index product determined the starting date for the study.

242
243 The impact of cyclones on leaf area was calculated by comparing the change in leaf area before and after the cyclone
244 in the affected area with changes before and after the cyclone in the reference area for each individual cyclone. In this
245 approach, the reference area serves as the control for the affected area, given that the reference area and the affected
246 area may have a different size, the adjusted Hedge's effect size (Rustad et al., 2001) can be used to calculate the effect
247 size of an individual cyclone on leaf area (**Eq. 1**). Using a reference area that is specific to each cyclone, seasonal

248 dynamics such as leaf phenology, are accounted for in the effect size. Effect size is thus a unitless quantifier that
 249 describes the mean change in state, obtained by normalizing the mean difference in leaf area with the standard
 250 deviation (**Eq. 1**). A positive or negative effect size value indicates, respectively, an increase or decrease in leaf area
 251 following the passage of a cyclone:

$$252 \quad ES = \frac{(\overline{LAI}_{bef} - \overline{LAI}_{aft})_{aff} - (\overline{LAI}_{bef} - \overline{LAI}_{aft})_{ref}}{\sigma}, \quad [1]$$

253 where ES is the event-based effect size for leaf area. The upper bar represents the mean of leaf area index in the
 254 reference (ref) or the affected (aff) area. The subscripts bef and aft denote the observation dates before and after the
 255 cyclone; σ denotes the standard deviation of all observations within the storm track. Given the 10-day frequency of
 256 the ESA leaf area index product, two leaf area index maps are used for the calculation of the effect size, one to
 257 characterize the leaf area index 1 to 10 days before the cyclone and the other to characterize the leaf area index 60 to
 258 70 days after the cyclone. To distinguish between the affected and reference areas the effect sizes were calculated for
 259 each event using the nine definitions. After applying the quality control criteria (see below) a different number of
 260 events was available for each definition (**Table A1**).

261 Starting the analysis from the actual storm tracks, as was the case in this study, allows for an unbiased assessment of
 262 the impact of cyclones on forests (Blanc and Strobl, 2016), in contrast to studies that attribute decreases in leaf area
 263 or related satellite-based indices to different disturbance agents (Ozdogan et al., 2014; Honkavaara et al., 2013;
 264 Forzieri et al., 2020) including cyclones (Takao et al., 2014). By design, the latter approach is not capable of
 265 identifying neutral or positive impacts of cyclones on leaf area. As positive effects were not limited to the cyclones
 266 from a low intensity class (**Fig. A3**), the intensity class had little explanatory power (**Table 1**) making a systematic
 267 bias towards positive effect sizes caused by low intensity cyclones unlikely. Given the 60-day time window, our
 268 method is more likely to be biased towards detecting no changes in leaf area than detecting positive or negative
 269 changes in leaf area.

270 A meaningful effect size relies on the change in the reference area to evaluate whether the change in leaf area in the
 271 affected area is faster, similar or slower. The way the effect size is calculated thus accounts for phenological changes
 272 in leaf area. If the reference area would not be used in the calculation of the effect size, the change in leaf area over
 273 the affected area would mostly represent leaf phenology especially if the 60-day window includes the start or the end
 274 of the growing season, and would thus be unsuitable to address the question at hand.

275 As this study aims to quantify changes in leaf area index, it could not make use of gap-filled leaf area index values
 276 which would level off such changes. Furthermore, calculating the effect size required leaf area index estimates before
 277 the passage of the cyclone in the reference and soon-to-be affected area and leaf area index estimates after the passage
 278 of the cyclone in the reference and affected area. The 60-day time frame was a compromise to avoid excessive data
 279

284 gaps in the leaf area index product when using the composite leaf area index product. Because the leaf area index
 285 product reports leaf area index values within a 60-day window, the analysis had to be refined so that this 60-day
 286 window never included the cyclone. The offset between the cyclone and a leaf area index observation from the
 287 composite leaf area index product was calculated by subtracting the date of the cyclone from the last observation date
 288 of the leaf area index composite data before the cyclone or the first observation date of the leaf area index composite
 289 data after the cyclone. Pixels with a negative offset indicated that the composite data were likely to include
 290 observations from both before and after the cyclone and were therefore discarded in the calculations of the effect size.

291
 292 The calculation of the effect size assumes having a similar leaf area index between the area that will become the
 293 affected area and the area that will become the reference area after the passage of a cyclone. If the absolute difference
 294 in leaf area index between the reference and the affected area was less than 10 %, the effect size calculated for this
 295 event was included in subsequent analyses. This can be formalized as:

$$296 \quad \left| \frac{\overline{LAI}_{bef,aff} - 1}{\overline{LAI}_{bef,ref}} \right| < 0.1 \quad [2]$$

297
 298 Where the 0.1 represents the 10 % threshold that was guided by the observed relationship between the remotely-sensed
 299 leaf area and its deviation to ground truth data for leaf areas of 5 m² m⁻² or below (Fig. 26 in Jorge, 2020). This quality
 300 control criterion reflects the idea that prior to the passage of a tropical cyclone, the LAI needs to be similar in what
 301 will become the reference and affected area. If not, changes in leaf area following the passage of the cyclone cannot
 302 be assigned to its passage.

303
 304 Following the passage of a tropical cyclone, a change in LAI of less than 10% before and after the passage of the
 305 cyclone was, in line with the quality control criterion, considered to be too small to be considered substantial. Such
 306 events were classified as cyclones with a neutral effect size. This classification was formalized as:

$$307 \quad |(\overline{LAI}_{bef} - \overline{LAI}_{aft})_{aff} - (\overline{LAI}_{bef} - \overline{LAI}_{aft})_{ref}| < 0.1 * (\overline{LAI}_{bef})_{ref} \quad [3]$$

311 **Multivariate analysis**

312 Each tropical cyclone was characterized by some cyclone characteristics: (1) latitude of landfall (degrees); (2) intensity
 313 of the tropical cyclone (m s⁻¹); (3) month of landfall; (4) maximum wind speed during passage over land (m s⁻¹); (5)
 314 affected area during passage over land (km²). Likewise, the area affected by the cyclone was characterized by: (6)
 315 accumulated rainfall on land 30 days prior to landfall of the cyclone (mm); (7) accumulated rainfall during passage
 316 over land (mm); (8) leaf area 30 days prior to landfall (m² m⁻²); (9) standardized precipitation evapotranspiration index
 317 (mm mm⁻¹) as a drought proxy; (10) change in standardized precipitation evapotranspiration index (mm mm⁻¹) and

318 (11) Pacific Japan index the month of landfall (Pa Pa^{-1}). These characteristics were calculated as the average along the
319 trajectory of the cyclone.

320
321 Characteristics 1 to 4 were retrieved from the Joint Typhoon Warning Center database as detailed in ‘Cyclone track
322 and track diameter’. Characteristics 5 and 7 were quantified from the analysis combining cyclone track, cyclone
323 diameter, and ERA5-Land reanalysis, as explained in ‘Area affected by individual cyclones’. Characteristics 6 and 7
324 were retrieved from the ERA5-Land reanalysis data for land (ECMWF, 2019). Characteristic 8 was taken from the
325 leaf area index analysis as explained in ‘Impact on leaf area of an individual cyclone’. For characteristics 9 and 10,
326 the standardized precipitation evapotranspiration index was used and combined with the cyclone masks created in the
327 ‘Area affected by the individual cyclone’. Characteristic 11, the Pacific Japan index, was calculated from ERA5 hourly
328 reanalysis (Hersbach et al., 2018). Details on the calculation of characteristics 9, 10, and 11 are provided in subsequent
329 sections.

330
331 Factor analysis (Grice, 2001) was used to reveal the collinearity among the selected variables in the prior conditions,
332 tropical cyclone characteristic group, and effect size (**Table A2**). The four main factors which explained 58% of the
333 variance, were classified into three groups (**Table 1**) using a decision tree (**Fig. A4**). Note that only the first and second
334 axis were used in the decision tree. The decision tree was created by means of the recursive partitioning approach with
335 a maximum of two levels and a minimum of 20 samples in each node provided by the R-rpart package (Therneau et
336 al., 2019).

337
338 **Drought analysis**

339 The standardized precipitation evapotranspiration index, is a proxy index for a drought that represents the climatic
340 water balance and was used to assess the drought of a forest soil before and after the passage of an individual tropical
341 cyclone. The standardized precipitation evapotranspiration index data between 1999 and 2018 were retrieved from the
342 Global Standardized Precipitation and Evapotranspiration Index Database (SPEIbase v2.6 (Beguería et al., 2014)),
343 which is based on the CRU TS v.4.03 dataset (Harris et al., 2020). In this study, the temporal resolution of the data
344 was preserved but the spatial resolution was regridded from the original half-degree to 1 km to match the resolution
345 of the ESA leaf area index product. The contribution of an individual tropical cyclone to ending a drought was
346 evaluated by comparing the standardized precipitation and evapotranspiration index from affected and reference areas
347 through the following equation:

$$348 \delta SPEI = (SPEI_{imon})_{aff} - (SPEI_{imon})_{ref} \quad [3]$$

350
351 where $\delta SPEI$ is the event-based change in standardized precipitation and evapotranspiration index. A positive or
352 negative $\delta SPEI$ respectively denotes an increase or decrease in available water resources following the passage of a
353 tropical cyclone. The subscription *imon* represents the integration time of available water resources in the calculation

354 of the standardized precipitation and evapotranspiration index either in the reference (*ref*) or the affected (*aff*) area
355 which are defined in the previous section. The same time window, i.e., 60-days, was applied for the calculation of
356 δ SPEI and event-based effect size for leaf area index. The surface state was considered to experience a dry spell when
357 the standardized precipitation and evapotranspiration index dropped below -1.0 in this study.

358

359 **Atmospheric analysis**

360 The Pacific Japan index was calculated by comparing the difference of the 3-month running mean atmospheric
361 pressure anomaly from Yokohama in Japan (35N, 155E) with Hengchun in Taiwan (22.5N, 125E) (Kubota et al.,
362 2016) with the 20 year climatology from 1999 to 2019. A monthly Pacific Japan index was used in this study and the
363 pressure data were retrieved from ERA5 (Hersbach et al., 2018). The Pacific Japan index for the month of the passage
364 of each tropical cyclone were stratified according to the impact (given by the effect size) of the cyclone on forest leaf
365 area. Mean absolute atmospheric pressure field and leaf area were calculated for those cyclones with a neutral effect
366 size on leaf area (**Fig. 3a**). Changes in pressure field and leaf area were calculated for both cyclones with a positive
367 and negative impact on leaf area (**Fig. 3b & c**).

368

369 **Acknowledgments**

370 We acknowledge the reviewers and the editors for advice on the methodology which improved the overall scientific
371 quality of this study. We thank M. J. McGrath, C. Yue, and B. Gardiner for providing their comments on the result of
372 this study during the early phase of this study. Y.Y.C. thank H.-H. Hsu for the discussion of analysing atmospheric
373 conditions, C.-H. Wu for the comments on considering the uncertainty of remote sensing data, respectively. Y.Y.C.
374 would like to thank the National Center for High-performance Computing (NCHC) for sharing its computational
375 resources and data storage facilities. Y.Y.C. was funded through the Ministry of Science and Technology (grant MOST
376 109-2111-M-001-011 and grant MOST 110-2111-M-001 -011). SL was partly funded through the H2020 project
377 HoliSoils (SEP-210673589) and the HE project INFORMA (101060309).

378

379 **Data availability**

380 R-Scripts and data for performing the analysis and creating the plots can be found at
381 https://github.com/ychenatsinca/LAI_STUDY_EA_V1/releases/tag/v1 and <https://doi.org/10.5281/zenodo.6459795>.
382 The database of event-based effect sizes, surface properties and cyclone properties for each of the 1262 events (i.e.,
383 140 \pm 41 unique tropical cyclones analysed for nine related definitions) can be accessed at:
384 <http://YYCdb.synology.me:5833/sharing/MqA4YFBHk>

385

386 **Author Contribution**

387 Y.Y.C. and S.L. designed the study. Y.Y.C. investigated and visualized the results. Y.Y.C. and S.L. contributed to the
388 interpretation of the results. S.L. wrote the original draft. S.L. and Y.Y.C. reviewed and edited the manuscript.

389

390 **Competing Interest Statement:**

391 The authors have the following competing interests: S.L. is an editorial board member of *Biogeosciences*.

392

393 **References**

394 Altman, J., Ukhvatkina, O. N., Omelko, A. M., Macek, M., Plener, T., Pejcha, V., Cerny, T., Petrik, P., Srutek, M.,
395 Song, J.-S., Zhmerenetsky, A. A., Vozmishcheva, A. S., Krestov, P.V., Petrenko, T. Y., Treydte, K., and Dolezal,
396 J.: Poleward migration of the destructive effects of tropical cyclones during the 20th century, *Proc. Natl. Acad.*
397 *Sci.*, 115, 11543–11548, <https://doi.org/10.1073/pnas.1808979115>, 2018.

398 Beguería, S., Vicente-Serrano, S. M., Reig, F., and Latorre, B.: Standardized precipitation evapotranspiration index
399 (SPEI) revisited: Parameter fitting, evapotranspiration models, tools, datasets and drought monitoring, *Int. J.*
400 *Climatol.*, 34, 3001–3023, <https://doi.org/10.1002/joc.3887>, 2014.

401 Blanc, E. and Strobl, E.: Assessing the impact of typhoons on rice production in the Philippines, *J. Appl. Meteorol.*
402 *Climatol.*, 55, 993–1007, <https://doi.org/10.1175/jamc-d-15-0214.1>, 2016.

403 Bushnell, J. M., Cherrett, R. C., and Falvey, R. J.: Annual Tropical Cyclone Report 2018, 147pp., 2018.

404 Chambers, J. Q., Fisher, J. I., Zeng, H., Chapman, E. L., Baker, D. B., and Hurtt, G. C.: Hurricane Katrina’s carbon
405 footprint on U.S. Gulf coast forests, *Science*, 318, 1107–1107, <https://doi.org/10.1126/science.1148913>, 2007.

406 Chang, C.-T., Lee Shaner, P.-J., Wang, H.-H., and Lin, T.-C.: Resilience of a subtropical rainforest to annual typhoon
407 disturbance: Lessons from 25-year data of leaf area index, *For. Ecol. Manage.*, 470–471, 118210,
408 <https://doi.org/10.1016/j.foreco.2020.118210>, 2020.

409 Chapin III, F. S., Matson, P. A., and Vitousek, P. M.: *Principles of Terrestrial Ecosystem Ecology*, 546pp.,
410 <https://doi.org/10.1007/978-1-4419-9504-9>, 2011.

411 Chen, Y.-Y., Gardiner, B., Pasztor, F., Blennow, K., Ryder, J., Valade, A., Naudts, K., Otto, J., McGrath, M. J.,
412 Planque, C., and Luysaert, S.: Simulating damage for wind storms in the land surface model ORCHIDEE-CAN
413 (revision 4262), *Geosci. Model Dev.*, 11, 771–791, <https://doi.org/10.5194/gmd-11-771-2018>, 2018.

414 Chen, Y., Sharma, S., Zhou, X., Yang, K., Li, X., Niu, X., Hu, X., and Khadka, N.: Spatial performance of multiple
415 reanalysis precipitation datasets on the southern slope of central Himalaya, *Atmos. Res.*, 250, 105365,
416 <https://doi.org/10.1016/j.atmosres.2020.105365>, 2021.

417 Chiu, C.-M., Chien, C.-T., Nigh, G., and Chung, C.-H.: Influence of climate on tree mortality in Taiwan (Taiwania
418 *cryptomerioides*) stands in Taiwan, *New Zeal. J. For. Sci.*, 48, <https://doi.org/10.1186/s40490-018-0111-0>, 2018.

419 Choi, K.-S., Wu, C.-C., and Cha, E.-J.: Change of tropical cyclone activity by Pacific-Japan teleconnection pattern in
420 the western North Pacific, *J. Geophys. Res. Atmos.*, 115, 1–13, <https://doi.org/10.1029/2010JD013866>, 2010.

421 Choi, K.-S., Kim, D.-W., and Byun, H.-R.: Relationship between summer drought of mid-latitudes in East Asia and
422 tropical cyclone genesis frequency in the Western North Pacific, in: *Advances in Geosciences (A 6-Volume Set)*,
423 edited by: Satake, K. and Wu, C.-C., World Scientific Publishing Co. Pte. Ltd., 1–13,
424 https://doi.org/10.1142/9789814355315_0001, 2011.

425 The Joint Typhoon Warning Center Tropical Cyclone Best-Tracks, 1945-2000:
426 <https://www.metoc.navy.mil/jtwc/products/best-tracks/tc-bt-report.html>, last access: 25June2019.

427 Curran, T. J., Brown, R. L., Edwards, E., Hopkins, K., Kelley, C., McCarthy, E., Pounds, E., Solan, R., and Wolf, J.:
428 Plant functional traits explain interspecific differences in immediate cyclone damage to trees of an endangered
429 rainforest community in north Queensland, *Austral Ecol.*, 33, 451–461, <https://doi.org/10.1111/j.1442->
430 9993.2008.01900.x, 2008.

431 Douglas, I.: Hydrological investigations of forest disturbance and land cover impacts in South–East Asia: a review,
432 *Philos. Trans. R. Soc. London. Ser. B Biol. Sci.*, 354, 1725–1738, <https://doi.org/10.1098/rstb.1999.0516>, 1999.

433 Dvorak, V. F.: Tropical cyclone intensity analysis using satellite data,
434 <https://repository.library.noaa.gov/view/noaa/19322>, 1984.

435 Dvorak, V. F., Smigielski, F. J., and States., U.: A workbook on tropical clouds and cloud systems observed in satellite
436 imagery, file://catalog.hathitrust.org/Record/002715963, 1990.

437 ECMWF: IFS Documentation CY45R1 - Part II: Data assimilation, in: IFS Documentation CY45R1, ECMWF,
438 <https://doi.org/10.21957/a3ri44ig4>, 2018.

439 ECMWF: ERA5-Land hourly data from 1981 to present, <https://doi.org/10.24381/cds.e2161bac>, 2019.

440 Eloy, C., Fournier, M., Lacoïnte, A., and Moulia, B.: Wind loads and competition for light sculpt trees into self-similar
441 structures, *Nat. Commun.*, 8, 1–11, <https://doi.org/10.1038/s41467-017-00995-6>, 2017.

442 ESA: Land Cover CCI Product User Guide Version 2, 105pp., 2017.

443 Forzieri, G., Pecchi, M., Girardello, M., Mauri, A., Klaus, M., Nikolov, C., Rüetschi, M., Gardiner, B., Tomaščík, J.,
444 Small, D., Nistor, C., Jonikavicius, D., Spinoni, J., Feyen, L., Giannetti, F., Comino, R., Wolynski, A., Pirotti, F.,
445 Maistrelli, F., Savulescu, I., Wurpillot-Lucas, S., Karlsson, S., Zieba-Kulawik, K., Strejczek-Jazwinska, P.,
446 Mokroš, M., Franz, S., Krejci, L., Haidu, I., Nilsson, M., Wezyk, P., Catani, F., Chen, Y.-Y., Luyssaert, S., Chirici,
447 G., Cescatti, A., and Beck, P. S. A.: A spatially explicit database of wind disturbances in European forests over
448 the period 2000–2018, *Earth Syst. Sci. Data*, 12, 257–276, <https://doi.org/10.5194/essd-12-257-2020>, 2020.

449 Grice, J. W.: Computing and evaluating factor scores., *Psychol. Methods*, 6, 430–450, <https://doi.org/10.1037/1082->
450 989X.6.4.430, 2001.

451 Harris, I., Osborn, T. J., Jones, P., and Lister, D.: Version 4 of the CRU TS monthly high-resolution gridded
452 multivariate climate dataset, *Sci. Data*, 7, 1–18, <https://doi.org/10.1038/s41597-020-0453-3>, 2020.

453 Hersbach, H., Bell, B., Berrisford, P., Biavati, G., Horányi, A., Muñoz Sabater, J., Nicolas, J., Peubey, C., Radu, R.,
454 Rozum, I., Schepers, D., Simmons, A., Soci, C., Dee, D., Thépaut, J.-N. H. H., Bell, B., Berrisford, P., Biavati, G.,
455 and Horányi, A. J.-N.: ERA5 hourly data on single levels from 1959 to present. Copernicus Climate Change
456 Service (C3S) Climate Data Store (CDS), <https://doi.org/10.24381/cds.adbb2d47>, 2018.

457 Honkavaara, E., Litkey, P., and Nurminen, K.: Automatic storm damage detection in forests using high-altitude
458 photogrammetric imagery, *Remote Sens.*, 5, 1405–1424, <https://doi.org/10.3390/rs5031405>, 2013.

459 Jorge, S.-Z.: Copernicus Global Land Operations “Vegetation and Energy,”
460 https://land.copernicus.eu/global/sites/cgls.vito.be/files/products/CGLOPS1_SQE2019_LAI300m-V1_I1.00.pdf,
461 2020.

462 Kaplan, J. and Demaria, M.: On the decay of tropical cyclone winds after landfall in the New England Area, *J. Appl.*
463 *Meteorol.*, 40, 280–286, [https://doi.org/10.1175/1520-0450\(2001\)040<0280:OTDOTC>2.0.CO;2](https://doi.org/10.1175/1520-0450(2001)040<0280:OTDOTC>2.0.CO;2), 2001.

464 Kubota, H., Kosaka, Y., and Xie, S. P.: A 117-year long index of the Pacific-Japan pattern with application to
465 interdecadal variability, *Int. J. Climatol.*, 36, 1575–1589, <https://doi.org/10.1002/joc.4441>, 2016.

466 Landsea, C. W.: Climate variability of tropical cyclones: Past, Present and Future, in: *Storms*, edited by: Pielke, R. A.
467 S. and Pielke, R. A. J., Routledge, New York, 220–241, 2000.

468 Lin, T.-C., Hamburg, S., Lin, K.-C., Wang, L.-J., Chang, C.-T., Hsia, Y.-J., Vadeboncoeur, M. A., Mabry McMullen,
469 C. M., and Liu, C.-P.: Typhoon disturbance and forest dynamics: Lessons from a Northwest Pacific subtropical
470 forest, 14, 127–143, <https://doi.org/10.1007/s10021-010-9399-1>, 2011.

471 Lin, T. C., Hogan, J. A., and Chang, C. Te: Tropical Cyclone Ecology: A Scale-Link Perspective, *Trends Ecol. Evol.*,
472 35, 594–604, <https://doi.org/10.1016/j.tree.2020.02.012>, 2020.

473 Louf, J. F., Nelson, L., Kang, H., Song, P. N., Zehnbaauer, T., and Jung, S.: How wind drives the correlation between
474 leaf shape and mechanical properties, *Sci. Rep.*, 8, 1–7, <https://doi.org/10.1038/s41598-018-34588-0>, 2018.

475 ECMWF Confluence Wiki: Implementation of IFS cycle 45r1:
476 <https://confluence.ecmwf.int/display/FCST/Implementation+of+IFS+cycle+45r1#ImplementationofIFScycle45r1-Tropicalcyclones>.
477 1-Tropicalcyclones.

478 Mabry, C. M., Hamburg, S. P., Lin Teng-Chiu, Horng, F. W., King, H. B., and Hsia, Y. J.: Typhoon disturbance and
479 stand-level damage patterns at a subtropical forest in Taiwan, *Biotropica*, 30, 238–250,
480 <https://doi.org/10.1111/j.1744-7429.1998.tb00058.x>, 1998.

481 Martins, J. P., Trigo, I., and Freitas, S. C. de: Copernicus Global Land Operations ”Vegetation and Energy” “CGLOPS-
482 1,” *Copernicus Glob. L. Oper.*, 1–93, 2020.

483 McDowell, N. G., Allen, C. D., and erson-Teixeira, K., Aukema, B. H., Bond-Lamberty, B., Chini, L., Clark, J. S.,
484 Dietze, M., Grossiord, C., Hanbury-Brown, A., Hurtt, G. C., Jackson, R. B., Johnson, D. J., Kueppers, L., Lichstein,
485 J. W., Ogle, K., Poulter, B., Pugh, T. A. M., Seidl, R., Turner, M. G., Uriarte, M., Walker, A. P., and Xu, C.:
486 Pervasive shifts in forest dynamics in a changing world, *Science*, 368, <https://doi.org/10.1126/science.aaz9463>,
487 2020.

488 Negrón-Juárez, R., Baker, D. B., Zeng, H., Henkel, T. K., and Chambers, J. Q.: Assessing hurricane-induced tree
489 mortality in U.S. Gulf Coast forest ecosystems, *J. Geophys. Res.*, 115, G04030,
490 <https://doi.org/10.1029/2009JG001221>, 2010.

491 Negrón-Juárez, R., Baker, D. B., Chambers, J. Q., Hurtt, G. C., and Goosem, S.: Multi-scale sensitivity of Landsat
492 and MODIS to forest disturbance associated with tropical cyclones, *Remote Sens. Environ.*, 140, 679–689,
493 <https://doi.org/10.1016/j.rse.2013.09.028>, 2014.

494 Nitta, T.: Convective Activities in the Tropical Western Pacific and Their Impact on the Northern Hemisphere Summer
495 Circulation, *J. Meteorol. Soc. Japan. Ser. II*, 65, 373–390, https://doi.org/10.2151/jmsj1965.65.3_373, 1987.

496 Ozdogan, M., Vladimirova, N., Radeloff, V. C., Krylov, A., Wolter, P. T., and Baumann, M.: Landsat remote sensing
497 of forest windfall disturbance, *Remote Sens. Environ.*, 143, 171–179, <https://doi.org/10.1016/j.rse.2013.12.020>,
498 2014.

499 Rustad, L. E., Campbell, J. L., Marion, G. M., Norby, R. J., Mitchell, M. J., Hartley, A. E., Cornelissen, J. H. C.,
500 Gurevitch, J., Alward, R., Beier, C., Burke, I., Canadell, J., Callaghan, T., Christensen, T. R., Fahnestock, J.,
501 Fernandez, I., Harte, J., Hollister, R., John, H., Ineson, P., Johnson, M. G., Jonasson, S., John, L., Linder, S.,
502 Lukewille, A., Masters, G., Melillo, J., Mickelsen, A., Neill, C., Olszyk, D. M., Press, M., Pregitzer, K., Robinson,
503 C., Rygielwicz, P. T., Sala, O., Schmidt, I. K., Shaver, G., Thompson, K., Tingey, D. T., Verburg, P., Wall, D.,
504 Welker, J., and Wright, R.: A meta-analysis of the response of soil respiration, net nitrogen mineralization, and
505 aboveground plant growth to experimental ecosystem warming, *Oecologia*, 126, 543–562,
506 <https://doi.org/10.1007/s004420000544>, 2001.

507 Takao, G., Saigusa, N., Yamagata, Y., Hayashi, M., and Oguma, H.: Quantitative assessment of the impact of typhoon
508 disturbance on a Japanese forest using satellite laser altimetry, *Remote Sens. Environ.*, 156, 216–225,
509 <https://doi.org/10.1016/j.rse.2014.09.028>, 2014.

510 Tang, S., Lin, T.-C., Hsia, Y.-J., Hamburg, S. P., and Lin, K.-C.: Typhoon effects on litterfall in a subtropical forest,
511 *Can. J. For. Res.*, 33, 2184–2192, <https://doi.org/10.1139/x03-154>, 2003.

512 Therneau, T., Atkinson, B., and Ripley, B.: Rpart: Recursive partitioning for classification, regression and survival
513 trees., CRAN R package version 4.1-15, 2019.

514 Uriarte, M., Thompson, J., and Zimmerman, J. K.: Hurricane María tripled stem breaks and doubled tree mortality
515 relative to other major storms, *Nat. Commun.*, 10, 1–7, <https://doi.org/10.1038/s41467-019-09319-2>, 2019.

516 Verger, A., Baret, F., and Weiss, M.: Near real-time vegetation monitoring at global scale, *IEEE J. Sel. Top. Appl.*
517 *Earth Obs. Remote Sens.*, 7, 3473–3481, <https://doi.org/10.1109/JSTARS.2014.2328632>, 2014.

518 Virost, E., Ponomarenko, A., Dehandschoewercker, Quéré, D., and Clanet, C.: Critical wind speed at which trees break,
519 *Phys. Rev. E*, 93, <https://doi.org/10.1103/PhysRevE.93.023001>, 2016.

520 Wang, H.-C., Wang, S.-F., Lin, K.-C., Lee Shaner, P.-J., and Lin, T.-C.: Litterfall and Element Fluxes in a Natural
521 Hardwood Forest and a Chinese-fir Plantation Experiencing Frequent Typhoon Disturbance in Central Taiwan,
522 *Biotropica*, 45, 541–548, <https://doi.org/10.1111/btp.12048>, 2013.

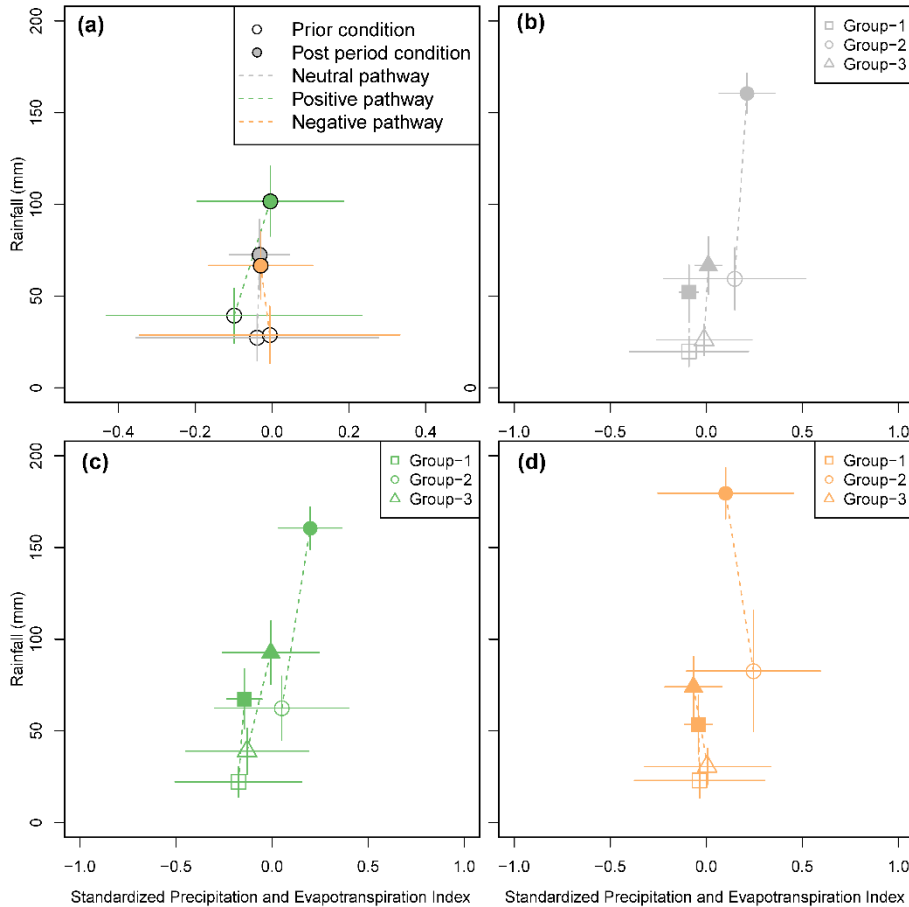
523 Willoughby, H. E. and Rahn, M. E.: Parametric representation of the primary hurricane vortex. Part I: Observations
524 and evaluation of the Holland (1980) model, *Mon. Weather Rev.*, 132, 3033–3048,
525 <https://doi.org/10.1175/MWR2831.1>, 2004.

526 WMO: Global Guide to Tropical Cyclone Forecasting, 399pp., 2017.

527 Yoo, J., Kwon, H.-H. H., So, B.-J. J., Rajagopalan, B., and Kim, T.-W. W.: Identifying the role of typhoons as drought
528 busters in South Korea based on hidden Markov chain models, *Geophys. Res. Lett.*, 42, 2797–2804,
529 <https://doi.org/10.1002/2015GL063753>, 2015.

530

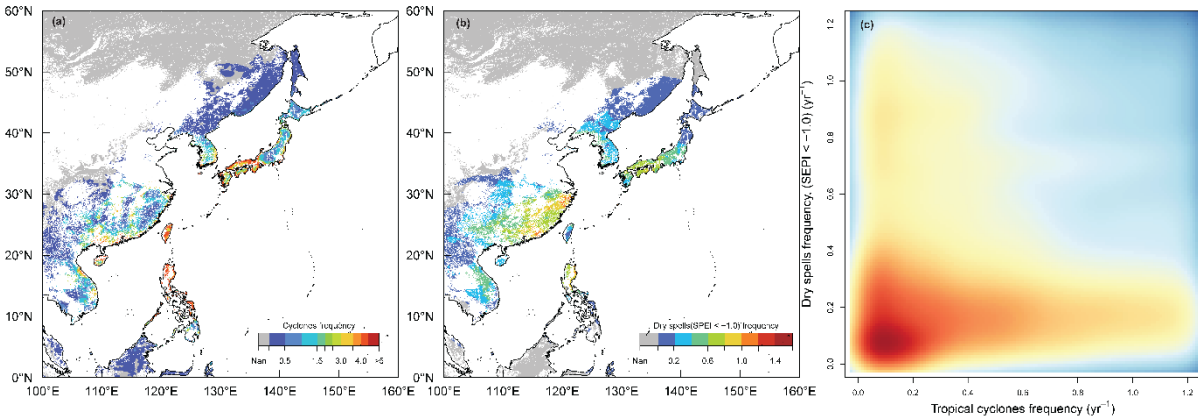
531 **Figures and Tables**



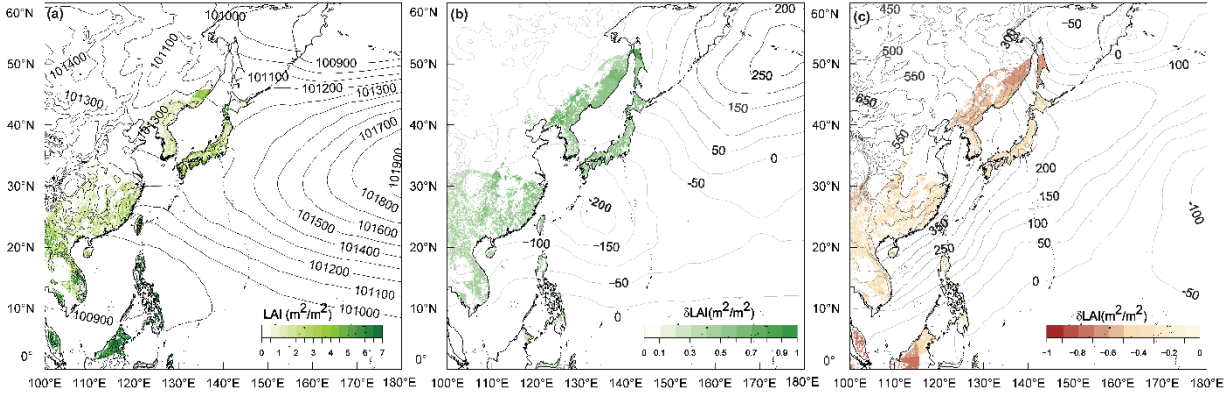
532
 533 **Figure 1.** Changes in standardized precipitation and evapotranspiration index following the precipitation brought by
 534 tropical cyclones. **(a)** Response in standardized precipitation and evapotranspiration index following the passage of a
 535 tropical cycle that resulted in a decrease (orange), no change (grey), or increase (green) in leaf area. Increasing leaf
 536 area was observed in forests that experienced a dry spell prior to the passage of a cyclone that brought sufficient
 537 precipitation to end the dry spell. **(b-d)** Response in standardized precipitation and evapotranspiration index following
 538 the passage of a tropical cycle that resulted in no change (grey; **b**) an increase (green; **c**), and a decrease (orange; **d**)
 539 in leaf area for the three cyclone groups (**Table 1**). Similar responses hint at similar mechanisms underlying the
 540 responses in leaf area irrespective of the cyclone group. The dashed line indicates the pathway moving from the
 541 condition prior to the condition after the passage of the cyclones.

542

543



544
 545 **Figure 2.** Spatial distribution of cyclone frequency, frequency of dry spells with a standardized precipitation and
 546 evaporation index below -1, and their correlation. (a) Return frequency (yr^{-1}) of tropical cyclones between 1999 and
 547 2018 following a combined wind-precipitation definition considering three diameters to define the width of the storm
 548 track (definition 3a in **Table A1**). (b) Return frequency (yr^{-1}) of dry spells between 1999 and 2018 following the same
 549 definition. (c) Smoothed density plot of the relationship ($r \sim 0.11$) between the return frequency of cyclones and dry
 550 spells. High-density regions are shown in warm colours compared to the cold colours used to indicate low-density
 551 regions. The density plot is based on all nine definitions for affected area (**Table A1**).
 552

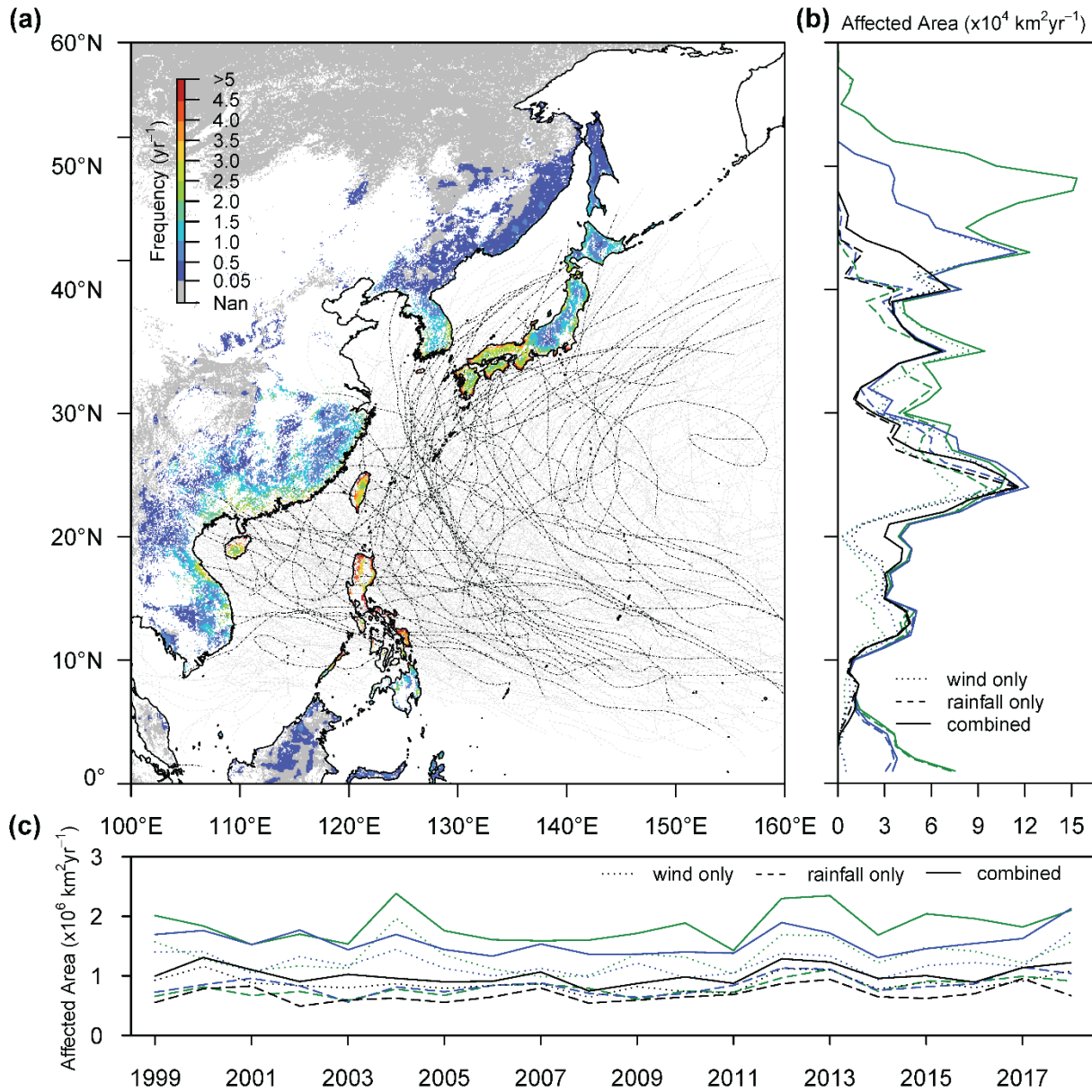


553
 554 **Figure 3.** Pressure fields (Pa) and changes therein in the month of the passage of a tropical cyclone for cyclones that
 555 had a neutral, positive, or negative impact on the leaf area ($m^2 m^{-2}$) of forests. Effect sizes are based on the definition
 556 that uses three times the cyclone diameter and wind speed to identify the affected and reference areas (definition 3a
 557 in **Table A1**) (a) Mean atmospheric pressure and leaf area prior to the passage of a tropical cyclone that had a neutral
 558 impact on forest leaf area. (b) Changes in mean atmospheric pressure and leaf area between cyclones with a neutral
 559 and positive effect on leaf area. (c) Changes in mean atmospheric pressure and leaf area between cyclones with a
 560 neutral and negative effect on leaf area.
 561

562 **Table 1.** Median and standard deviation for five cyclone characteristics and six surface characteristics mainly prior to
563 the passage of the 140±41 tropical cyclones that passed the quality checks. Cyclone groups 1 to 3 were the outcome
564 of a decision tree (**Fig. A4**) that classified the four main factors of factorial analysis of the land surface characteristics,
565 cyclone characteristics, and effect sizes to identify collinearity (**Table A2**). The column labelled with ANOVA shows
566 the p-value of an ANOVA test to test for significant differences between cyclone groups.
567

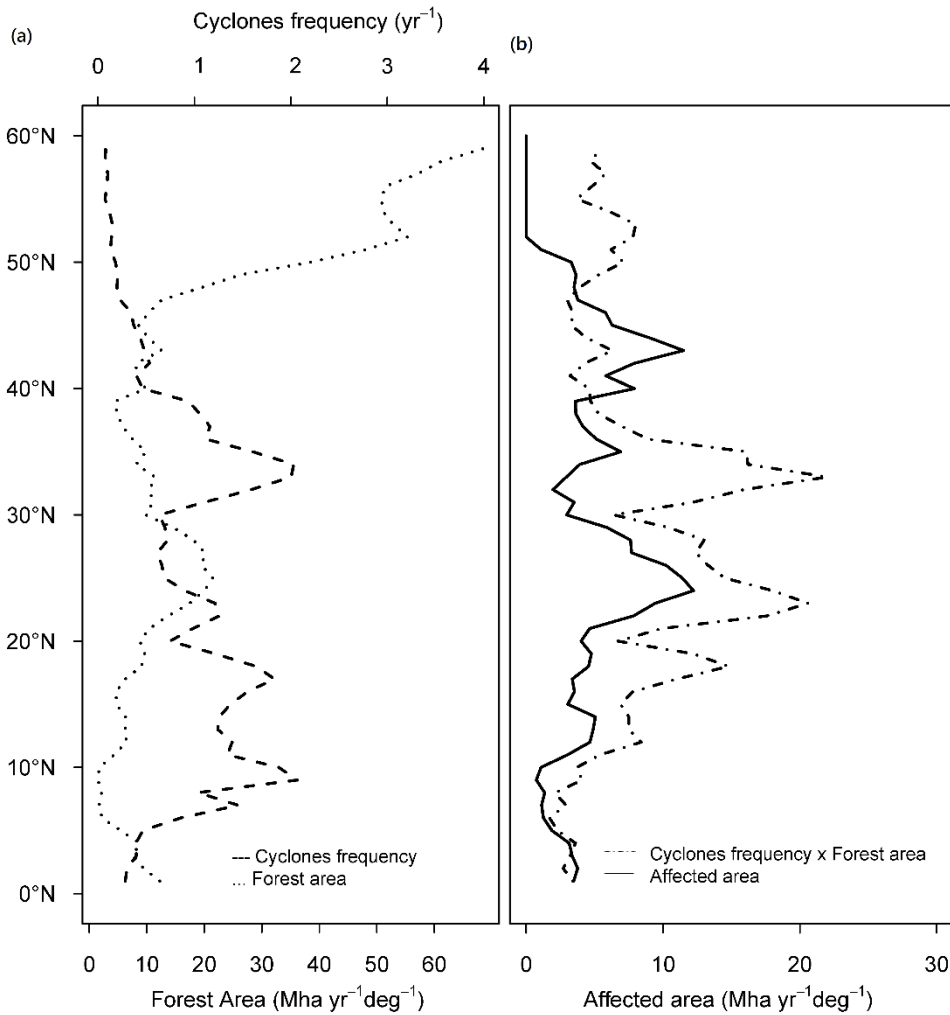
	Characteristic	Cyclone group 1	Cyclone group 2	Cyclone group 3	ANOVA
Tropical cyclone characteristics	Latitude of landfall (degrees)	33.6 ± 4.2	23.3 ± 6.9	22.9 ± 8.7	<0.05
	Affected area during passage over land (km ²)	65,008 ± 19,010	5,944 ± 5,324	15,960 ± 11,598	<0.05
	Accumulated rainfall during passage over land (mm)	41.7 ± 33.9	100.8 ± 22.9	23.0 ± 31.2	<0.05
	Maximum wind speed during passage over land (m s ⁻¹)	12.5 ± 2.0 (a)	7.2 ± 2.8 (b)	12.1 ± 2.7 (a)	<0.05
	Intensity of the tropical cyclone, gusts (m s ⁻¹)	29.2 ± 9.9	20.8 ± 9.5	25.0 ± 10.3	<0.05
Surface conditions prior to the cyclone	Pacific Japan index (Pa Pa ⁻¹)	-0.24 ± 0.09	-0.15 ± 0.11	-0.05 ± 0.12	<0.05
	Prior accumulated rainfall (30 days prior to landfall (mm))	30.1 ± 23.3	54.7 ± 38.0	16.5 ± 17.2	<0.05
	Month of landfall	8.0 ± 1.1 (a)	8.0 ± 2.0 (a)	8.0 ± 2.7 (a)	0.42
	Prior leaf area index (30 days prior to landfall (m ² m ⁻²))	4.50 ± 0.9	4.02 ± 0.82	3.56 ± 0.96	<0.05
	Drought state (SPEI, 30 days prior to landfall (mm mm ⁻¹))	-0.12 ± 0.60 (a)	0.06 ± 0.71 (b)	-0.13 ± 0.64 (a)	<0.05
	Delta SPEI (mm mm ⁻¹)	0.13 ± 0.53	0.32 ± 0.62	0.04 ± 0.40	<0.05
Effect on forest leaf area	Positive effect size (%)	62	48	19	
	Negative effect size (%)	10	8	24	
	Neutral effect size (%)	28	44	57	
Share in Tropical Cyclones (%)		23	18	59	

568



570
 571 **Figure A1.** Spatial and temporal patterns of potential forest damage by tropical cyclones in East Asia. (a) Return
 572 frequency (yr^{-1}) of tropical cyclones between 1999 and 2018 following a combined wind-precipitation definition
 573 considering three diameters to define the width of the storm track (definition 3a in **Table A1**). Since 1999, $2,240,000$
 574 $\pm 690,000 \text{ km}^2$ of forest in the study region experienced conditions that may have resulted in cyclone-driven damage,
 575 at least once every decade. No less than $540,000 \pm 260,000 \text{ km}^2$, including 70 % of the tropical forest in the region,
 576 experienced potentially damaging conditions at least once per year, and are thus classified as being under chronic
 577 wind stress. Forests unlikely to have experienced a tropical cyclone between 1999 and 2018 are shaded in grey. For
 578 land locations shown in white, the forest is not the dominant land cover. The dot-dashed lines show the cyclone tracks

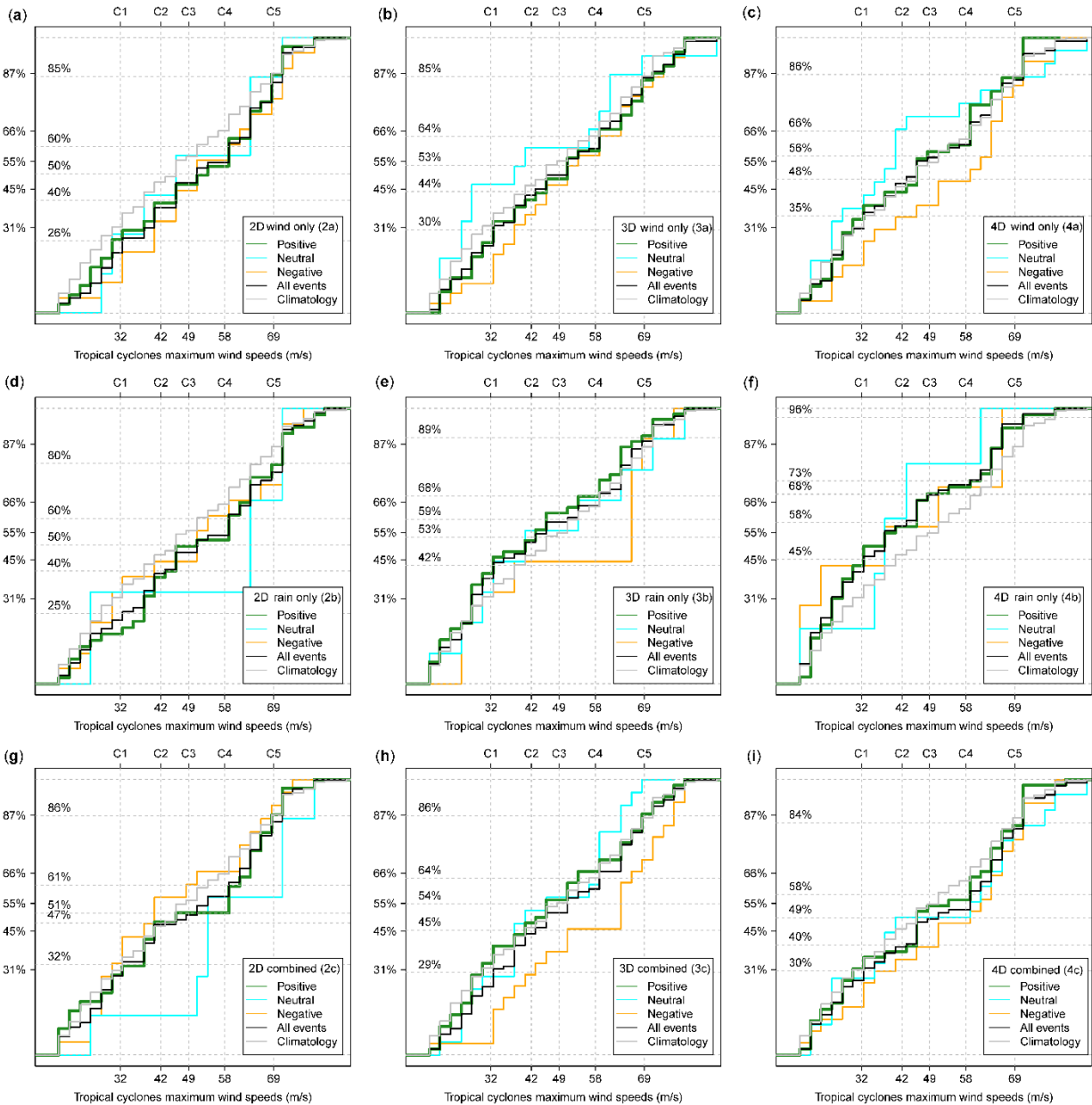
579 between 1999 and 2018. The black lines indicate the events that passed the quality control criteria used in this study.
580 (b) Latitudinal gradients of potentially damaged forest area ($\text{km}^2 \text{ yr}^{-1}$) between 1999 to 2018 for all nine definitions
581 of affected area. Damage potential is the outcome of an interplay between cyclone frequency, cyclone intensity, and
582 the presence of forests. The different definitions of affected area (**Table A1**) consistently show a high potential for
583 forest damage over island and coastal regions located between 10 and 35 degrees north. This high potential is largely
584 driven by the frequency of tropical cyclones (**Fig. A2**), i.e., two or more cyclones making landfall per year. Depending
585 on how the affected area is defined, there is a second region located between 40 and 50 degrees north with a high
586 potential for storm damage. In this region, the potential damage is the outcome of the high forest cover resulting in a
587 strong dependency on the assumed width of the storm track (**Fig. A2**). (c) Temporal dynamics of the total potentially
588 damaged forest area ($\text{km}^2 \text{ yr}^{-1}$) for all nine definitions of affected area. Irrespective of the definition of the affected
589 area, the coefficient of variation of the between-year variation in potentially damaged areas ranged from 15 to 20%.
590 Excluding the four most powerful typhoons that occurred in the region since 1999 changed the average coefficient of
591 variation from 17 to 16%. This suggests that the most powerful typhoons make only a small contribution to the total
592 annually potentially affected area in the region. Likewise, a recent literature review reported that 66 % of the research
593 papers in this area have examined the effects of only about 6% of the most powerful cyclones (Lin et al., 2020). The
594 relatively small contribution of those events to the potential damage area suggests that in regions with frequent tropical
595 storms, disturbance ecology would benefit from broadening its scope by examining the effects and recovery of a
596 representative sample of tropical cyclones, rather than focusing on the most devastating events.
597



598

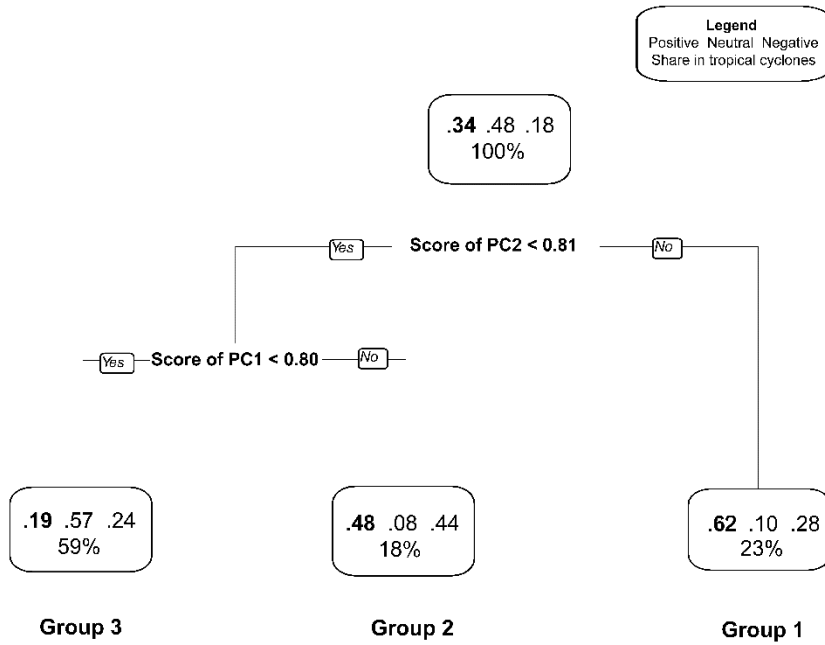
599 **Figure A2.** Contribution of return frequency and forest cover to the affected area: (a) the zonal average of forest
 600 coverage (dotted line; km²) and the return frequency (dashed line; yr⁻¹) of tropical cyclones from 0 to 60 degrees N
 601 averaged over Eastern Asia, as defined in this study; (b) Zonal average of the interaction between return frequency
 602 and forest cover, calculated by multiplying the return frequency with the forest cover (dot-dash line; km² yr⁻¹) and the
 603 estimated zonal average of the annual affected forest area (full line; km² yr⁻¹). Correlations between return frequency
 604 and affected area (Pearson correlation coefficient = -0.35, p-value < 0.01, n = 60), forest cover and affected area
 605 (Pearson correlation coefficient = 0.089, p-value = 0.5, n = 60) and frequency x cover and affected area (Pearson
 606 correlation coefficient = 0.44, p-value < 0.01, n = 60). The latter thus correlates best with the zonal variation in the
 607 affected area and was therefore shown in subplot b. Results are shown for affected areas defined as locations within
 608 an area extending to three times the cyclone width for which the wind exceeded a threshold (definition 3a in Table
 609 **A1**).

610



611
 612 **Figure A3.** Cumulative distribution of tropical cyclones as a function of their maximum intensity for the nine
 613 definitions of affected area speeds used in this study. The cumulative distribution for the census of 580 tropical cyclones
 614 recorded for the study period is shown left of the y-axis for class I (31%), class II (45%), class III (55%), class IV
 615 (66%) and class V (87%) cyclones. The numbers shown on the right of the y-axis represent the cumulative distribution
 616 of the sample of the 580 events following a specific definition. Panel (a) shows wind only for 2 diameters, (b) wind
 617 only for 3 diameters, (c) wind only for 4 diameters, (d) rain only for 2 diameters, (e) rain only for 3 diameters, (f) rain
 618 only for 4 diameters, (g) wind or rain for 2 diameters, (h) wind or rain for 3 diameters, and (i) wind or rain for 4
 619 diameters as detailed in Table S1. The intensity distribution for tropical cyclones with a negative effect size is shown
 620 in orange, for tropical cyclones with a neutral effect size is shown in blue, and for tropical cyclones with a positive

621 effect size in green. The black solid line shows the distribution for the specific definition ($n = 140 \pm 41$ cyclones
622 depending on the definition). The grey solid line shows the distribution of the 580 events that occurred between 1999
623 to 2018. Small deviations between the grey and the black line suggest that the sample well represented the 580 cyclones
624 in terms of their intensity class. The maximum wind speed of category I cyclones is between 32ms^{-1} and 42ms^{-1} ,
625 between 42ms^{-1} and 49ms^{-1} for category II, between 49ms^{-1} and 58ms^{-1} for category III, between 58ms^{-1} and 69ms^{-1}
626 for category IV, and exceeding 69ms^{-1} for category V. In East Asia, tropical cyclones of intensity class III or higher
627 are called typhoons.
628



629
 630 **Figure A4.** Decision tree proposing three groups of cyclones based on cyclone characteristics, surface properties
 631 mainly prior to the passage of the cyclone, and its effect on leaf area in the affected compared to the reference area.
 632 Each box shows the fractions of negative (left), neutral (middle) and positive (right) effect sizes (see also **Table 1**).
 633 The number of events is listed as the percentage of the total number of events in the random tree (n=1262). The first
 634 two principal components PC1 and PC2 (Table A2) were used to create a two-layer decision tree.

635 **Table A1.** Criteria for distinguishing between the affected and reference areas following the passage of an individual
636 cyclone and the number of events according to each specific definition. Group 1 groups definitions are based on wind
637 speed, group 2 definitions are based on precipitation, and group 3 definitions are based on both wind speed and
638 precipitation. All three definitions include an estimate of the storm path based on a multiple of the reported storm
639 diameter. Column A denotes the number of events for which data were lacking so that the effect size could not be
640 calculated; column B denotes the number of events for which all required data were available; column C denotes the
641 subset of B for which the data passed the quality control; ES refers to effect size. A total of 580 unique tropical cyclones
642 were considered in this study.

Group	Affected area	Reference area	A	B	C	Negative effect size	Neutral effect size	Positive effect size
1.a	> 8 m s ⁻¹ and <2 diameters	< 8 m s ⁻¹ and <2 diameters	342	238	105	22	51	32
1.b	> 10 m s ⁻¹ and <3 diameters	< 10 m s ⁻¹ and <3 diameters	305	275	182	38	97	47
1.c	> 12 m s ⁻¹ and <4 diameters	< 12 m s ⁻¹ and <4 diameters	291	289	183	31	92	60
2.a	> 60 mm and <2 diameters	< 60 mm and <2 diameters	338	242	115	19	51	45
2.b	> 80 mm and <3 diameters	< 80 mm and <3 diameters	315	265	129	11	59	59
2.c	> 100 mm and <4 diameters	< 100 mm and <4 diameters	311	269	86	9	32	45
3.a	(> 8 m s ⁻¹ or > 60 mm) and <2 diameters	(< 8 m s ⁻¹ or < 60 mm) and < 2 diameters	352	228	103	25	45	33
3.b	(> 10 m s ⁻¹ or > 80 mm) and <3 diameters	(< 10 m s ⁻¹ or < 80 mm) and < 3 diameters	304	276	188	38	95	55
3.c	(> 12 m s ⁻¹ or > 100 mm) and <4 diameters	(< 12 m s ⁻¹ or < 100 mm) and < 4 diameters	288	292	171	35	83	53
Mean			316	264	140	25	67	48
Std			22	22	41	11	25	10
Mean (%)			54	46	24	18	48	34
Std (%)			4	4	7	8	18	7

643

644

645 **Table A2.** Loadings of each characteristic on four principal axes and collinearity between variables within the same
646 group. Given the exploratory nature of this analysis, a factor loading of 0.6 was used as a cut-off and those exceeding
647 that level are highlighted in boldface.

	Characteristic	PC1	PC2	PC3	PC4
Tropical cyclone characteristics	Latitude of landfall (degrees)	-0.62	0.18	0.48	0.00
	Affected area during passage over land (km ²)	0.82	0.02	0.15	0.11
	Accumulated rainfall during passage over land (mm)	-0.15	0.86	0.14	0.07
	Maximum wind speed during passage over land (m s ⁻¹)	-0.32	0.24	0.05	0.22
	Intensity of the tropical cyclone, gusts (m s ⁻¹)	-0.34	0.60	-0.45	0.08
Surface conditions prior to the cyclone	Pacific Japan index (Pa Pa ⁻¹)	0.01	0.11	-0.54	-0.03
	Prior accumulated rainfall (30 days prior to landfall (mm))	0.73	0.06	0.21	-0.10
	Month of landfall	0.29	0.11	0.76	-0.02
	Prior leaf area index (30 days prior to landfall (m ² m ⁻²))	-0.30	-0.75	0.13	0.06
	Drought state (SPEI, 30 days prior to landfall (mm mm ⁻¹))	0.22	-0.01	0.02	-0.81
	Delta SPEI (mm mm ⁻¹)	0.28	0.07	0.05	0.77
	Effect size	0.41	0.37	0.12	0.16
The proportion of total variance		19%	16%	12%	11%

648